Empagliflozin reduces renal lipotoxicity in experimental Alport syndrome

Authors:

Mengyuan Ge[1,2], Judith Molina[1,2], Jin-Ju Kim[1,2], Shamroop K Mallela[1,2], Anis Ahmad[3], Javier Varona Santos[1,2], Hassan Al-Ali[1,2], Alla Mitrofanova[1,2], Kumar Sharma[4], Flavia Fontanesi[5], Sandra Merscher[1,2], Alessia Fornoni*[1,2]

Affiliations:

1. Katz Family Division of Nephrology and Hypertension, Department of Medicine, University of Miami Miller School of Medicine, Miami, Florida.
2. Peggy and Harold Katz Family Drug Discovery Center, University of Miami Miller School of Medicine, Miami, Florida.
3. Department of Radiation Oncology, University of Miami Miller School of Medicine, Miami, Florida.
4. Center for Precision Medicine, School of Medicine, University of Texas Health San Antonio, San Antonio, Texas.
5. Department of Biochemistry and Molecular Biology, University of Miami, Miami, Florida.

***Corresponding author**

Alessia Fornoni, MD, PhD at the Katz Family Division of Nephrology and Hypertension and Peggy and Harold Katz Family Drug Discovery Center, University of Miami, 1580 NW 10th Ave, Miami, FL 33136, USA (email: afornoni@med.miami.edu; tel.+1-305-243-7745; fax+1-305-243-3506).

Abstract

Sodium-glucose cotransporter-2 inhibitors (SGLT2i) are anti-hyperglycemic agents that prevent glucose reabsorption in proximal tubular cells. SGLT2i improves renal outcomes in both diabetic and non-diabetic patients, indicating it may have beneficial effects beyond glycemic control. Here, we demonstrate that SGLT2i affects energy metabolism and renal lipotoxicity in experimental

Alport syndrome (AS). *In vitro*, we found that SGLT2 protein expression levels in human and mouse podocytes were similar to tubular cells. Newly established immortalized podocytes from Col4a3 knockout mice (AS podocytes) accumulate lipid droplets along with increased apoptosis when compared to wildtype podocytes. Treatment with SGLT2i empagliflozin reduces lipid droplet accumulation and apoptosis in AS podocytes. Empagliflozin inhibits the utilization of glucose/pyruvate as a metabolic substrate in AS podocytes. *In vivo*, we demonstrate that empagliflozin reduces albuminuria and prolongs the survival of AS mice. Empagliflozin-treated AS mice show decreased serum blood urea nitrogen and creatinine levels in association with reduced triglyceride and cholesterol ester content in kidney cortices when compared to AS mice. Lipid accumulation in kidney cortices correlates with the decline in renal function. In summary, empagliflozin reduces renal lipotoxicity and improves kidney function in experimental AS in association with the energy substrates switch from glucose to fatty acids in podocytes.

Keywords: Alport syndrome; SGLT2 inhibitor; lipid; energy substrate.

Introduction

Alport syndrome (AS) is a hereditary disease of glomerular basement membranes caused by mutations in collagen type IV genes A3, A4 and A5 (Barker et al., 1990; Gross et al., 2016; Longo et al., 2002). AS is characterized by renal fibrosis with progression to end-stage renal disease in young adult life (Barker et al., 1990; Grunfeld, 2000; Williamson, 1961). Though early treatment with angiotensin-converting enzyme inhibitors (ACEi) was shown to reduce proteinuria and delay disease progression in both retrospective (Gross et al., 2012) and prospective (Boeckhaus et al., 2022) studies, there is no specific treatment to prevent renal failure in patients with AS.

Sodium-glucose cotransporter 2 inhibitors (SGLT2i), initially developed for the treatment of patients with type 2 diabetes (T2D), were recently found to protect from kidney and cardiovascular outcomes in both diabetic and non-diabetic patients with chronic kidney disease (CKD) (Heerspink et al., 2020). SGLT2 is most abundantly expressed in the apical brush border membrane of the proximal tubule, where it plays a key role in renal glucose reabsorption (Vallon et al., 2011). SGLT2i selectively block SGLT2, thereby enhancing urinary glucose excretion and reducing glycemia (DeFronzo, Norton, & Abdul-Ghani, 2017; Novikov & Vallon, 2016; Vallon & Thomson, 2017). While the major mechanism for renoprotection is thought to involve the tubuloglomerular feedback and glomerular hemodynamics (Cherney et al., 2014), SGLT2i may also modulate key metabolic pathways linked to CKD progression. In response to increased glycosuria, the body engenders a metabolic adaption to enhance the usage of fat for energy production (Ferrannini et al., 2016). Additional studies have also shown that SGLT2i enhances β-oxidation in the liver (Wallenius et al., 2022) and improves liver fat deposition in patients with T2D and fatty liver disease (Kuchay et al., 2018; Shibuya et al., 2018). Similarly, SGLT2i lowers the cardiac content of cardiotoxic lipids in obese diabetic rats (Aragon-Herrera et al., 2019). These observations suggest a possible link between SGLT2i and lipid metabolism. We and others have demonstrated that the accumulation of both cholesterol esters and fatty acids in podocytes and tubular cells contributes to the pathogenesis of AS (Ding et al., 2018; Kim et al., 2021; Mitrofanova

et al., 2018; Wright et al., 2021), indicating that reducing the lipid content in the kidney may potentially reduce lipotoxicity-mediated renal injury in AS.

Although all cells in the kidney are high energy-demanding, the metabolic substrates for ATP production are cell type-dependent (Console et al., 2020). Renal proximal tubular cells in particular use free fatty acids as the preferred fuel, whereas inhibition of fatty acid oxidation (FAO) renders tubular cells susceptible to cell death and lipid accumulation (Kang et al., 2015). Podocytes usually rely on glucose for energy production, while fatty acids are used as an alternative substrate (Abe et al., 2010; Brinkkoetter et al., 2019). Interestingly, a recent study demonstrated SGLT2 expression in podocytes and its expression was modulated by exposure to albumin, although the functional relevance of SGLT2 expression in podocytes is unknown (Cassis et al., 2018). With this study, we aimed at investigating if SGLT2i affects energy metabolism in both podocytes and tubular cells in experimental AS.

Results

SGLT2 is expressed in human podocytes and immortalized podocytes established from wildtype (WT) and AS mice. Immunohistochemistry in normal human kidney sections demonstrated both glomerular and proximal tubules expression of SGLT2 (Figure 1A). Using Western blot analysis, we demonstrate similar level of SGLT2 protein expression levels in cultured human podocytes when compared to HK2 tubular cells. Mouse liver lysate, HepG2 liver cancer cells and kidney lysate from $SGLT2^{-/-}$ mouse were used as the negative controls (Figure 1B). To study the effect of SGLT2i in an experimental model of non-diabetic kidney disease, we developed immortalized podocytes and tubular cell lines established from $SV40^{+/-}$;$Col4a3^{+/+}$ (immorto-WT) and $SV40^{+/-}$;$Col4a3^{-/-}$ (immorto-AS) mice. The expression of the podocyte-specific marker Synaptopodin (SYNPO) and of the tubule-specific marker Aquaporin 1 (AQP1) was confirmed in podocyte and tubular cell lines, respectively (Figure 1-Figure supplement 1). We found a similar level of SGLT2 protein expression in both tubular cells and podocytes (Figure 1C). SGLT2

expression in both AS tubular cells and podocytes was not different from WT controls (Figure 1D).

Treatment of AS podocytes with empagliflozin reduces lipid droplet accumulation and apoptosis. We previously described that AS podocytes are characterized by increased apoptosis and lipid droplet (LD) accumulation when compared to WT podocytes (Kim et al., 2021; Liu et al., 2020). To further evaluate whether SGLT2i can reduce lipotoxicity in podocytes as well as in tubular cells isolated from AS mice, immortalized WT and AS podocytes and tubular cells were treated with empagliflozin or vehicle. We found increased cytotoxicity, although not significant, in AS compared to WT tubular cells. However, SGLT2i significantly decreases cytotoxicity in empagliflozin-treated compared with vehicle-treated AS tubular cells (Figure 2A). No differences in apoptosis and lipid droplet accumulation were observed in any of the groups (Figure 2B,E). As expected, AS podocytes showed increased cytotoxicity, apoptosis, and intracellular LD when compared to WT podocytes (Figure 2C,D,F). Empagliflozin treatment significantly reduced apoptosis and intracellular LD, but not cytotoxicity in AS podocytes (Figure 2C,D,F). Representative picture of Nile red staining revealed fewer LD per cell in empagliflozin-treated compared with vehicle-treated AS podocytes (Figure 2H), suggesting empagliflozin ameliorates lipotoxicity in AS podocytes. Interestingly, we observed a positive correlation between LD accumulation and apoptosis (Figure 2G).

Empagliflozin inhibits the utilization of pyruvate as a metabolic substrate in AS podocytes. To investigate if empagliflozin affects metabolic substrate preferences, endogenous cellular and coupled substrate-driven respiration were measured by high-resolution respirometry. Endogenous respiration measured in intact cells was not altered in either AS tubular cells or podocytes compared to WT (Figure 3A,B). Cells were then permeabilized with digitonin and substrates for fatty acids-driven and NADH-driven respiration were provided sequentially. No difference in oxygen consumption rate (OCR) was detected between WT and AS tubular cells in response to fatty acids. However, AS tubular cells show elevated respiration after the addition of NADH-linked substrates. Treatment of empagliflozin did not affect the respiration of AS tubular

cells independently of the substrate (Figure 3A). In contrast to tubular cells, AS podocytes showed a slightly but significant increase in FAO-linked OCR compared to WT podocytes, which could be due to the increase in intracellular lipid accumulation. This increase was maintained upon empagliflozin treatment and showed a tendency to increase, though not significant (Figure 3B). Moreover, addition of NADH-linked substrates to WT and AS podocytes increased OCR to approximately the double of the value recorded in presence of FAO-linked substrates, in agreement with podocytes preferential use of glucose oxidation for ATP production. Interestingly, NADH-linked respiration in AS podocytes was inhibited by treatment with empagliflozin (Figure 3B). To confirm the inhibitory effect of empagliflozin on NADH-driven respiration, we repeated the assay by measuring directly NADH-driven respiration without addition of fatty acids. A similar change was observed (Figure 3-Figure supplement 1A,B). Taken together, these data suggest that in podocytes established from AS mice, empagliflozin may induce a metabolic remodeling characterized by a reduction in glucose oxidation and a switch toward the use of alternative substrates for ATP production. To further characterize the adaptation to energy sources in AS podocytes, pyruvate dehydrogenase (PDH) activity was measured. PDH is an enzyme that converts glycolysis-derived pyruvate to acetyl-CoA and increases its influx into the tricarboxylic acid (TCA) cycle (Zhang, Hulver, McMillan, Cline, & Gilbert, 2014). PDH plays a central role in the reciprocal regulation of glucose and lipid oxidation (Zhang et al., 2014). We found that PDH activity was reduced in AS podocytes by Empagliflozin treatment (Figure 3C), suggesting a switch to the consumption of fatty acids as energy fuel.

Empagliflozin prolongs survival of AS mice. To investigate if empagliflozin can improve survival in mice with non-diabetic renal disease which typically die from renal failure, AS mice were fed an empagliflozin-supplemented chow (70 mg/kg) or a regular diet starting at 4 weeks of age for 6 weeks. Mice with experimental AS start developing proteinuria at 4 weeks of age, followed by death at 8-9 weeks of age. We found that empagliflozin extended the lifespan of AS mice by about 22% compared to untreated AS mice (Figure 4A). Blood glucose was measured at

8 weeks of age and no difference was observed in empagliflozin-treated compared to untreated AS mice (Figure 4B). These data suggest that the ability of empagliflozin to prolong the survival of AS mice is independent from its anti-hyperglycemic effects.

Empagliflozin improves renal function in a mouse model of Alport syndrome. To study the effects of SGLT2 inhibitors on the renal outcome, AS mice were fed empagliflozin-supplemented chow starting at 4-weeks of age for 4 weeks, and the renal phenotype was compared to AS mice fed a regular diet. Ramipril, an ACEi and used as a standard of care for patients with AS, was also used alone or in combination with empagliflozin. At 4-weeks of age, ramipril was added to the drinking water and/or mice were fed with an empagliflozin-supplemented chow as indicated. Mice on the different regimens were compared with AS mice fed a regular diet. All mice were sacrificed at 8-week of age. Empagliflozin, ramipril and the empagliflozin + ramipril (E+R) combination significantly reduced the albumin-to-creatinine ratio (ACR) and prevented body weight loss in AS mice (Figure A,B). Empagliflozin, ramipril and E+R significantly reduced blood urea nitrogen (BUN) and creatinine levels in AS mice (Figure 5 C,D). Unlike what has been observed in patients enrolled in DAPA-CKD, addition of empagliflozin to standard of care (SOC) ramipril did not confer additional renoprotection, and overall, no difference across treatment groups was observed. Glomeruli of AS mice exhibited significant mesangial matrix expansion (Figure 5E) as determined by Periodic acid-Schiff (PAS) staining and significantly increased fibrosis as determined by Picrosirius red staining (Figure 5F), which were reduced by the treatment of empagliflozin, ramipril and E+R. Empagliflozin, ramipril and E+R treatment of AS mice also prevented podocyte loss as suggested by similar podocyte numbers, as indicated by increased Wilms tumor 1 (WT1)-positive cells per glomerulus, in treated AS compared to WT mice (Figure 5G).

Empagliflozin prevents renal lipid accumulation in experimental Alport syndrome. To investigate whether empagliflozin prevents lipid accumulation in kidney cortices of AS mice, Oil Red O (ORO) staining was performed. We found an increased number of LD-positive glomeruli

in AS mice, while the number of LD-positive glomeruli in all treatment groups was similar to WT mice (Figure 6A). We then extracted lipids from kidney cortices to investigate the composition of specific lipids and found increased cholesterol ester (CE) and triglyceride contents in AS compared to WT mice (Figure 6B,D), similar to what we previously reported (Kim et al., 2021). Interestingly, though all treatment groups showed a decreased CE content in kidney cortices, only Empagliflozin and E+R reduced triglycerides levels. The total cholesterol content was similar in all five groups (Figure 6C). We previously demonstrated a correlation between lipid accumulation and renal function decline in experimental models of metabolic and non-metabolic kidney disease (Ducasa et al., 2019; Ge et al., 2021; Wright et al., 2021). Similarly, we found a positive correlation of the CE, triglyceride content in kidney cortices with ACR, serum BUN, and creatinine levels (Figure 6E-J).

Discussion

In the present study, we investigate the mechanisms by which empagliflozin, an SGLT2i, affects the usage of glucose and fatty acids as energy substrates in podocytes and tubular cells as well as the effects of empagliflozin on lipotoxicity-induced cell injury and renal function decline. The expression of SGLT2 in podocytes has been previously reported by Cassis et al (Cassis et al., 2018), suggesting that podocytes can be a potential target of SGLT2i. Similarly, we demonstrate that SGLT2 protein is expressed in human kidney cortex, cultured human podocytes, as well as healthy and diseased mouse podocytes (Figure 1). We also show that SGLT2i reduces LD accumulation (Figure 2) and glucose/pyruvate-driven respiration (Figure 3) in immortalized podocytes established from AS mice. *In vivo*, we demonstrate for the first time that empagliflozin reduces renal lipotoxicity and prevents kidney disease progression in an experimental model of AS.

Renal lipotoxicity contributes to the pathogenesis of several forms of kidney disease (Ducasa et al., 2019; Pedigo et al., 2016; Yoo et al., 2015). We previously demonstrated that impaired

cholesterol efflux in podocytes plays a critical pathogenic role in diabetic kidney disease (DKD) (Ducasa et al., 2019; Merscher-Gomez et al., 2013) as well as in diseases of non-metabolic origin, including AS (Kim et al., 2021; Mitrofanova et al., 2018), where we have also observed altered free fatty acids metabolism. Others have reported that defective FAO is associated with lipid deposition and fibrosis in kidney tubules (Kang et al., 2015), and contributes to disease progression in AS (Ding et al., 2018). In this study, we utilized immortalized podocytes and tubular cells newly established from AS and WT mice. Proximal tubular cells are a known target of SGLT2i. Here, we aimed at investigating if podocytes and tubular cells change their preferences with regard to their metabolic fuel in response to SGLT2i. In the kidney, podocytes highly rely on glucose as the substrate for ATP production (Abe et al., 2010), while tubular cells use free fatty acid as the preferred energy source (Kang et al., 2015). Therefore, a reduction of glucose availability by SGLT2i may trigger the utilization of alternative energy substrates, such as lipids (Osataphan et al., 2019). To study the effect of SGLT2i on energy substrate switch, we first investigated whether SGLT2i exercises a protective effect on immortalized podocytes and tubular cells derived from AS mice. We demonstrate that AS podocytes have increased cytotoxicity and apoptosis when compared to WT podocytes (Figure 2). Empagliflozin treatment protected AS podocytes from apoptosis but not cytotoxicity. On the other hand, AS tubular cells did not show increased apoptosis but were found to exhibit a tendency to increased cytotoxicity when compared to WT tubular cells. Tubular cytotoxicity was significantly reduced by empagliflozin treatment. The apparent discrepancy between cytotoxicity and apoptosis could be explained by the fact that apoptosis is a coordinated and energy-reliant process that involves the activation of caspases, while cell death characterized by loss of cell membrane integrity (which was measured in our cytotoxicity assay) is energy-independent (Cummings & Schnellmann, 2004), therefore the two processes can take place independently, sequentially, as well as concurrently (Elmore, 2007). Interestingly, we observed a similar trend with regard to LD accumulation. We found a significantly increased number of LDs in AS podocytes compared to WT podocytes, which was reduced by

empagliflozin treatment. However, no difference in LD accumulation was observed in tubular cells (Figure 2), suggesting that the mechanisms leading to LD accumulation in podocytes in AS are cell-specific. As podocytes but not tubular cells in AS are in contact with an abnormal glomerular basement membrane, the possibility that the LD accumulation is the result of a cross talk between matrix and lipid metabolism is possible, as it was recently suggested by others (Romani et al., 2019). As far as the mechanisms linking a similar trend in LD accumulation and apoptosis, it was reported that lipids such as triglyceride, cholesterol, fatty acids and ceramide can directly induce caspase activation, leading to programmed cell death (Huang & Freter, 2015). The exact mechanism by which lipotoxicity induce apoptosis warrants further investigations.

To test the preference of energy substrate in association with AS and empagliflozin treatment, we measured cellular respiration by high-resolution respirometry (Figure 3). After permeabilizing the cells, we sequentially added different substrates and observed their direct effect on oxygen consumption. WT and AS tubular cells consume the same amount of oxygen in presence of FAO-linked substrates. However, AS tubular cells respire more following the addition of NADH-linked substrates. While not the major source of renal energy, glucose oxidation is crucial in tubular function (Ross, Espinal, & Silva, 1986). Elevated NADH-linked respiration in AS tubular cells may suggest an increased demand for alternative substrates in this cell type under disease conditions. Empagliflozin does not affect tubular cell respiration independently of the substrate used in the assay. However, empagliflozin treatment of AS podocytes inhibits NADH-linked respiration and appears to promote a shift in substrate utilization for ATP production. The accumulation of LD in AS podocytes could lead to an increase in the availability of fatty acids and contribute to the elevated FAO-linked respiration observed in these cells. Given that podocytes rely more on glucose oxidation and are therefore more vulnerable to glucose deprivation, it is feasible to speculate that empagliflozin only affects podocyte respiratory metabolism and not that of tubular cells.

While the major mechanisms by which SGLT2i reduces albuminuria is thought to be linked to a

modulation of the tubulo-glomerular feedback resulting in improved glomerular hyperfiltration (Mabillard & Sayer, 2020), it is possible that additional mechanisms are also involved. Several studies have demonstrated that SGLT2i has a remarkable effect on lipid metabolism *in vivo*. For example, SGLT2 inhibition modulates renal lipid metabolism in db/db mice (Wang et al., 2017), ameliorates obesity in high-fat diet-fed animal models by improving FAO (Wei et al., 2020; Yokono et al., 2014), and reduces the cardiotoxic lipids in the hearts of diabetic fatty rats (Aragon-Herrera et al., 2019). In this study, we demonstrate that empagliflozin treatment protects from renal disease progression and expands the life span of AS mice. We furthermore demonstrate that empagliflozin not only improves kidney function (Figure 5) but also significantly reduces intrarenal lipid accumulation (Figure 6) in AS mice. To allow for comparison to the SOC, the ACEi ramipril was also included in our study in order to determine whether a combination of empagliflozin and ramipril would have a superior effect to ramipril. We show that treatment of AS mice with both ramipril and empagliflozin is not superior in preserving renal function when compared to treatment with ramipril alone. While this is not consistent with the findings reported in patients with DKD, the very sizable effect of ramipril in experimental AS may account for the inability to report additional renoprotective effects of empagliflozin. Interestingly, we found that empagliflozin or the combined treatment of empagliflozin and ramipril reduces triglyceride content in the kidney of AS mice, while ramipril did not have any effect on the renal triglyceride content but affected esterified cholesterol content, suggesting that the effect of ACEi and SGLT2i on renal lipid metabolism may differ. More importantly, we identified a strong correlation between lipid accumulation (CE, triglyceride) in kidney cortices and the decline in renal function (albuminuria, serum BUN and creatinine), which is similar to our previous findings in experimental AS, DKD and FSGS (Ducasa et al., 2019; Ge et al., 2021; Wright et al., 2021). These data suggest that the renal protection of empagliflozin in AS may at least in part be mediated by its ability to modulate renal lipid metabolism. It is interesting to note that while podocyte-specific glucose transporter (GLUT) 4 deficient podocytes are characterized by morphology change which may be mediated by the lack of nutrient (Guzman et

al., 2014), GLUT4-deficient mice are protected from diabetic nephropathy. The beneficial effect of GLUT4 deficiency and SGLT2 inhibition may both be interpreted by deprivation of nutrients such as glucose. Further studies will be needed to understand the impact of renal lipid content in affected patients and to determine if renoprotection conferred by SGLT2i may be monitored through non-invasive measures of fat content such as Dixon magnetic resonance imaging (Gaborit et al., 2021).

Our study has several limitations. First, we did not study empagliflozin's off-target effect on other transporters such as sodium-hydrogen exchanger (NHE) 1 in the heart or NHE3 in the kidney (McGuire et al., 2021). It is possible that these pathways are also involved. However, recent study shows that empagliflozin does not inhibit NHE1 in the heart (Chung et al., 2021), and the way SGLT2i inhibit the NHE isoforms in the kidney remains to be proven (De Pascalis, Cianciolo, Capelli, Brunori, & La Manna, 2021). In addition, *in vitro* experiments were performed using immortalized podocytes and tubular cells established from AS and WT mice. While these cells are very similar to primary cells, they may exhibit some changes in protein expression and function. However, the *in vivo* study using an experimental model of non-metabolic kidney disease (AS mice) supports our hypothesis.

In summary, our study demonstrates that empagliflozin reduces renal lipotoxicity and improves kidney function in experimental AS. This beneficial effect is associated with a shift in the use of energy substrates from glucose to fatty acids in podocytes. Lipid accumulation in kidney cortices correlates with kidney disease progression, therefore reducing renal lipid content by empagliflozin and other agents may represent a novel therapeutic strategy for the treatment of patients with AS. Results obtained from this study may allow us to better define the mechanisms leading to SGLT2i-mediated renoprotection in non-diabetic kidney disease.

Methods

Animal studies

Phenotypic analysis of mice

Col4a3$^{-/-}$ mice (a model of AS) are in a 129X1/SvJ background and were purchased from Jackson Laboratory (129-Col4a3^{tm1Dec}/J, stock #002908). Mice were fed empagliflozin-supplemented chow (70 mg/kg) versus a regular diet starting at 4 weeks of age. Ramipril was added to the drinking water at a concentration that would lead to a daily uptake of 10 mg/kg body weight (Kim et al., 2021). Five groups of mice were examined: WT + placebo, AS + placebo, AS + empagliflozin, AS + ramipril and AS + empagliflozin + ramipril. Both male and female mice were used. Mice were sacrificed at 8 weeks and analyzed as described below.

Urinary albumin-to-creatinine ratios

Morning spot urine samples were collected bi-weekly. Urinary albumin-to-creatinine ratios were determined using the Mouse Albumin ELISA Kit (Bethyl Laboratories, Montgomery, TX) and Creatinine LiquiColor (Stanbio, Boerne, TX). Albuminuria values are expressed as µg albumin per mg creatinine.

Serology

Blood samples were collected and serum creatinine was determined by tandem mass spectrometry at the UAB-UCSD O'Brian Core Center (University of Alabama at Birmingham) as previously described (Takahashi, Boysen, Li, Li, & Swenberg, 2007). Serum BUN was analyzed in the Comparative Laboratory Core Facility of the University of Miami.

Oil red-O staining

Four µm kidney cortices optimal cutting temperature (OCT) compound embedded sections were incubated with 100 µl freshly prepared Oil Red O solution (Electron Microscopy Science, Hatfield, PA) for 15 minutes and counterstained with Hematoxylin Harris solution (VWR, 10143-606) for 5 min to detect lipid deposition. Images were examined under a light microscope (Olympus BX41, Tokyo, Japan), and quantified by the percentage of LD-positive glomeruli.

Podocyte Wilms tumor 1 (WT1) staining

To measure podocyte number per glomerulus, glomerular sections embedded in OCT were stained with a WT1 antibody (Santa Cruz Biotechnology, Dallas, TX, sc-192, 1:300), followed by a secondary antibody (Invitrogen, Waltham, MA, A-11008, 1:500) and Mounting Medium with DAPI (Vectorlabs, Newark, CA, H-1200). Images were acquired using Olympus IX81 confocal microscope (Tokyo, Japan) coupled with a 60x oil immersion objective lens and images were processed using Fiji/Image J. 5-10 glomeruli per mouse were quantified.

Kidney histology analysis

Perfused kidneys were fixed in 10% formalin and paraffin-embedded, and then cut into 4 µm thick sections. Periodic acid-Schiff (PAS) staining was performed to investigate mesangial expansion following a standard protocol. The mesangial expansion was visualized under a light microscope (Olympus BX41, Tokyo, Japan) and 20 glomeruli per section were scored by semi-quantitative analysis (scale 0-5), performed in a blinded manner. Picrosirius Red staining was performed to measure fibrosis. Paraffin-embedded sections were deparaffinized with xylene and a graded alcohol series. Sections were rinsed and stained for 1 hour with Picrosirius Red in saturated aqueous picric acid. Sections were examined under a light microscope (Olympus BX41, Tokyo, Japan), followed by analysis with Fiji/Image J.

Lipid extraction

Kidney cortices were homogenized in a buffer containing 50 mM pH 7.4 potassium phosphate and cOmplete Protease Inhibitor Cocktail tablet (Roche, Indianapolis, IN, 1 pill in 10 ml buffer) by sonication for 20s, twice, on ice. Total lipids were extracted from homogenates using hexane:isopropanol (3:2) and placed in a mixer (1000 rpm) for 30 min. The mixed homogenate was then spun at top speed, lipids contained in the supernatants were collected, and pellets were disrupted by 2 sequential lipid extractions. Total lipids were then pooled and dried using a speed vacuum at 37 °C and reconstituted with 100 µl isopropanol:NP-40 (9:1). Proteins were extracted from the pellets using 8 M Urea, 0.1% SDS, and 0.1M NaOH. Extracted lipids were used for

determining total cholesterol, cholesterol ester and triglyceride contents, and normalized to protein concentrations.

Triglyceride (TG) assay

The TG content was determined using Triglyceride Colorimetric Assay Kit (Cayman, Ann Arbor, MI) following the manufacturer's protocol. TG standards and lipid samples from above-mentioned extraction were added into a 96 well plate. The reaction was initiated by adding 150 µl enzyme buffer to each well. Absorbance at 540 nm was measured using a SpectraMax M5 plate reader (Molecular Devices, San Jose, CA).

Cholesterol assay

Cholesterol assays were performed using the Amplex Red Cholesterol Assay Kit (ThermoFisher Scientific, Waltham, MA) following the manufacturer's instructions with some modifications (Ge et al., 2021). Total cholesterol and cholesterol ester were quantified using a direct enzymatic method (Mizoguchi, Edano, & Koshi, 2004) and fluorescence was read at 530/580 nm. SpectraMax M5 plate reader (Molecular Devices, San Jose, CA) was used.

Immunohistochemistry

Four µm kidney sections were heated at 65 °C for 1 hour and deparaffinized in xylene, followed by rehydration in decreasing concentrations of ethanol (two washes in 100% ethanol, two washes in 95%, one wash in 70%, one wash in 50%, and three wash in TBS). Antigen retrieval was performed for 30 min in citrate buffer (Sigma-Aldrich, St. Louis, MO, C9999, 1:10). Sections were incubated with 3% hydrogen peroxidase (Sigma-Aldrich, St. Louis, MO, H1009, 1:10) for 20 min and incubated with a blocking reagent (Vector Laboratories, Newark, CA, SP-5035) for 1 hour at room temperature. Sections were then incubated with primary antibody SGLT2 (Santa Cruz Biotechnology, Dallas, TX, sc-393350, 1:100) overnight at 4 °C. Incubation with biotin-labeled secondary antibody (Vector Laboratories, Newark, CA, BA-2000, 1:200) was performed at room temperature for 1 hour, followed by incubation with avidin-biotin peroxidase complex (Vector Laboratories, Newark, CA, PK-6100) and DAB substrate kit (Vector Laboratories, Newark, CA,

SK-4100). Counterstain was performed with hematoxylin for 5 min, followed by dehydration in increasing concentrations of ethanol. Sections were examined under a light microscope (Olympus BX41, Tokyo, Japan).

Establishment and culture of conditionally immortalized mouse podocyte and tubular cell lines

To establish immortalized mouse podocyte and tubular cell lines, $Col4a3^{+/-}$ mice were bred with the immorto-mice carrying a temperature-sensitive T-antigen transgene ($SV40^{+/-}$) (Charles River, Wilmington, MA, CBA/CaxC57BL/10-H-2Kb-tsA58) (Jat et al., 1991) to generate double heterozygous littermates, which were then crossed to generate $SV40Tg^{+/-}$;$Col4a3^{-/-}$ (immorto-AS) and $SV40Tg^{+/-}$;$Col4a3^{+/+}$ (immorto-WT) (Kim et al., 2021; Liu et al., 2020). Glomeruli and tubules were isolated from 9 weeks old immorto-WT and -AS mice by differential sieving as previously described (Mundel et al., 1997; Terryn et al., 2007). Immortalized cell lines were cultured at 33 °C in RPMI growth medium (containing 10% FBS,1% penicillin/streptomycin, 100 U/ml IFNγ) under permissive condition, then thermo-shifted to 37 °C non-permissive condition in the absence of IFNγ. Immortalized mouse podocyte and tubular cell lines were characterized by Western blot analysis using podocyte and tubular cell markers. Cultured cells were incubated with 500 nM empagliflozin (Selleckchem, Houston, TX) or dimethylsulfoxide in growth medium for 48 h.

Western blot analysis

Cell lysates were prepared using 3-[(3-cholamidopropyl)dimethylammonio]-1-propanesulfonic (CHAPS) acid buffer. Protein concentration was measured with the bicinchoninic acid (BCA) reagent (Thermo Scientific, Waltham, MA). 20-30 µg of protein extract was loaded onto 4 to 20% SDS-polyacrylamide gel electrophoresis (SDS-PAGE) gels (Bio-Rad, Hercules, CA) and transferred to Immobilon-P PVDF membranes (Bio-Rad, Hercules, CA). Western blot analysis was performed using a standard protocol and the following primary antibodies: SGLT2 (Santa Cruz Biotechnology, Dallas, TX, sc-393350, 1:500), SYNAPTOPODIN (Santa Cruz Biotechnology, Dallas, TX, sc-21537, 1:1,000), AQP1 (Proteintech, Rosemont, IL, 20333-1-AP,

1:2000), GAPDH (Sigma-Aldrich, St. Louis, MO, CB1001, 1:10,000); or secondary antibodies: anti-mouse IgG horseradish peroxidase (HRP) (Promega, Madison, WI, W402B, 1:10,000), anti-rabbit IgG HRP (Promega, Madison, WI, W401B, 1:10,000) or anti-goat IgG HRP (Promega, Madison, WI, V805A, 1:10,000). Signal was detected with Radiance ECL (Azure, Dublin, CA) using Azure c600 Imaging System.

Cytotoxicity and apoptosis assay

Cytotoxicity and apoptosis assays were performed using the ApoTox-Glo Triplex assay (Promega, Madison, WI) according to the manufacturer's protocol. Fluorescence and luminescence were measured on a SpectraMax i3x multi-mode microplate reader (Molecular Devices, San Jose, CA).

Lipid droplet quantification

Cultured cells were fixed with 4% paraformaldehyde (PFA) and 2% sucrose and then stained with Nile red (Sigma-Aldrich, St. Louis, MO) and HCS Cell Mask Blue (Invitrogen, Waltham, MA) according to the manufacturer's protocols. Images were acquired using the Opera high content screening system (20x confocal lens) and lipid droplets intensity per cell was determined using the Columbus Image Analysis System (Perkin Elmer, Waltham, MA) (Liu et al., 2020).

Cellular respiration measurements

Oxygen consumption rate (OCR) was measured using a high-resolution respirometer (O2k-Fluo-Respirometer, Oroboros Instruments, Innsbruck, Austria) filled with 2 mL of mitochondrial respiration buffer (MiR05, containing 0.5 mM EGTA, 3 mM $MgCl_2 \cdot 6H_2O$, 60 mM K-lactobionate, 20 mM Taurine, 10 mM KH_2PO_4, 20 mM HEPES, 110 mM Sucrose, 1 g/l fatty acid-free BSA) at 37ºC, following the Substrate-Uncoupler-Inhibitor-Titration (SUIT)-002 protocol with some modifications. Specifically, $1x10^6$ suspended cells were immediately placed into the chamber and continuously mixed by a stirrer at 750 rotations per minute. O_2 consumption in nearly diffusion-tight closed chambers is calculated in real-time by polarographic oxygen sensors. First, endogenous respiration was measured in intact cells. For substrate-driven respiration, cells were

permeabilized with 2.5 ug/ml digitonin (optimal digitonin concentration for podocytes and tubular cells was established prior following the SUIT-010 protocol) and supplemented with 2.5 mM ADP. FAO-linked substrates (0.5 mM octanoylcarnitine plus 0.1 mM malate) were then added to the chamber using a Hamilton microsyringe, and the coupled FA-driven OCR was measured. Finally, 2 mM malate, 5 mM pyruvate and 10 mM glutamate were added to initiate coupled NADH-linked respiration, and the additive effect of NADH-driven OCR was measured. Mitochondrial outer membrane integrity was tested by addition of 10 uM cytochrome *c*. Respiration was inhibited by the addition of 100 mM sodium azide, which is a specific mitochondrial complex IV (CIV) inhibitor. Cell respiration was recorded as pmol O_2 consumed for 1 s and normalized to cell numbers.

Pyruvate dehydrogenase activity assay

Pyruvate dehydrogenase (PDH) activity in cells was determined using PDH Colorimetric Assay Kit (BioVision, Milpitas, CA) according to manufacturer's protocol. $1x10^6$ cells were used. Absorbance at 450 nm was measured using a SpectraMax M5 plate reader (Molecular Devices, San Jose, CA).

Statistics

For each statistical test, biological sample size (n), and *p*-value are indicated in the corresponding figure legends. All values are presented as mean ± SD. Statistical analysis was performed using Prism GraphPad 7 software. Significant outliers were determined by GraphPad outlier calculator and excluded from further statistical analysis. Animals were grouped according to genotypes then randomized, and investigators were blinded for the analyses. When comparing two groups, a two-tailed Student's t-test was performed. Otherwise, results were analyzed using One-way ANOVA followed by Holm-Sidak's multiple comparison. A *p*-value less than 0.05 was considered statistically significant. Only data from independent experiments were analyzed.

Study Approval

All studies involving mice were approved by the Institutional Animal Care and Use Committee (IACUC) at the University of Miami. The University of Miami (UM) has an Animal Welfare

Assurance on file with the Office of Laboratory Animal Welfare, NIH (A-3224-01, effective November 24, 2015). Additionally, UM is registered with the US Department of Agriculture Animal and Plant Health Inspection Service, effective December 2014, registration 58-R-007. As of October 22, 2013, the Council on Accreditation of the Association for Assessment and Accreditation of Laboratory Animal Care (AAALAC International) has continued UM's full accreditation.

Author contributions

MG performed the *in vitro* and *in vivo* experiments, analyzed the data, and wrote the manuscript. JM performed some *in vitro* experiments. JJK established immortalized podocytes and tubular cells. JVS and HAA designed experiments related to lipid droplet determination. SKM, AA, AM and KS assisted with some of the *in vivo* and *in vitro* experiments. KS edited the manuscript. AF conceived the project, FF, SM designed and supervised the study, analyzed the data, and edited the manuscript. AF is the guarantor of this work and, as such, had full access to all the data in the study and takes responsibility for the integrity of the data and the accuracy of the data analysis.

Disclosure statement

AF and SM are inventors on pending (PCT/US2019/032215; US 17/057,247; PCT/US2019/041730; PCT/US2013/036484; US 17/259,883; US17/259,883; JP501309/2021, EU19834217.2; CN-201980060078.3; CA2,930,119; CA3,012,773,CA2,852,904) or issued patents (US10,183,038 and US10,052,345) aimed at preventing and treating renal disease. They stand to gain royalties from their future commercialization. AF is Vice-President of L&F Health LLC and is a consultant for ZyVersa Therapeutics, Inc. ZyVersa Therapeutics, Inc has licensed worldwide rights to develop and commercialize hydroxypropyl-beta-cyclodextrin from L&F Research for the treatment of kidney disease. AF also holds equities in Renal 3 River Corporation. SM holds indirect equity interest in, and potential royalty from, ZyVersa Therapeutics, Inc. by

virtue of assignment and licensure of a patent estate. AF and SM are supported by Aurinia Pharmaceuticals Inc. KS is founder of SygnaMap.

Acknowledgement

This project was supported by grants from National Institutes of Health [grant numbers R01DK117599, R01DK104753 and R01CA227493] to AF and SM, and the Miami Clinical Translational Science Institute [grant numbers U54DK083912, UM1DK100846, U01DK116101 and UL1TR000460] to AF. FF is supported by the Army Research Office [grant number W911NF-21-1-0359]. We thank Dr Volker Vallon for the kidney lysate from SGLT2$^{-/-}$ mice. A special thanks to the Katz family for supporting this study.

Data availability

All data generated or analyzed during this study are included in the manuscript and supporting files.

References

Abe, Y., Sakairi, T., Kajiyama, H., Shrivastav, S., Beeson, C., & Kopp, J. B. (2010). Bioenergetic characterization of mouse podocytes. *Am J Physiol Cell Physiol, 299*(2), C464-476. doi:10.1152/ajpcell.00563.2009

Aragon-Herrera, A., Feijoo-Bandin, S., Otero Santiago, M., Barral, L., Campos-Toimil, M., Gil-Longo, J., . . . Lago, F. (2019). Empagliflozin reduces the levels of CD36 and cardiotoxic lipids while improving autophagy in the hearts of Zucker diabetic fatty rats. *Biochem Pharmacol, 170*, 113677. doi:10.1016/j.bcp.2019.113677

Barker, D. F., Hostikka, S. L., Zhou, J., Chow, L. T., Oliphant, A. R., Gerken, S. C., . . . Tryggvason, K. (1990). Identification of mutations in the COL4A5 collagen gene in Alport syndrome. *Science, 248*(4960), 1224-1227.

Boeckhaus, J., Hoefele, J., Riedhammer, K. M., Nagel, M., Beck, B., Choi, M., . . . Gross, O. (2022). Lifelong effect of therapy in young patients with the COL4A5 Alport missense variant p.(Gly624Asp): a prospective cohort study. *Nephrol Dial Transplant*. doi:10.1093/ndt/gfac006

Brinkkoetter, P. T., Bork, T., Salou, S., Liang, W., Mizi, A., Ozel, C., . . . Huber, T. B. (2019). Anaerobic glycolysis maintains the glomerular filtration barrier independent of mitochondrial metabolism and dynamics. *Cell Rep, 27*(5), 1551-1566 e1555. doi:10.1016/j.celrep.2019.04.012

Cassis, P., Locatelli, M., Cerullo, D., Corna, D., Buelli, S., Zanchi, C., . . . Zoja, C. (2018). SGLT2 inhibitor dapagliflozin limits podocyte damage in proteinuric nondiabetic nephropathy. *JCI Insight, 3*(15). doi:10.1172/jci.insight.98720

Cherney, D. Z., Perkins, B. A., Soleymanlou, N., Maione, M., Lai, V., Lee, A., . . . von Eynatten, M. (2014). Renal hemodynamic effect of sodium-glucose cotransporter 2 inhibition in patients with type 1 diabetes mellitus. *Circulation, 129*(5), 587-597. doi:10.1161/CIRCULATIONAHA.113.005081

Chung, Y. J., Park, K. C., Tokar, S., Eykyn, T. R., Fuller, W., Pavlovic, D., . . . Shattock, M. J. (2021). Off-target effects of sodium-glucose co-transporter 2 blockers: empagliflozin does not inhibit Na+/H+ exchanger-1 or lower [Na+]i in the heart. *Cardiovasc Res, 117*(14), 2794-2806. doi:10.1093/cvr/cvaa323

Console, L., Scalise, M., Giangregorio, N., Tonazzi, A., Barile, M., & Indiveri, C. (2020). The link between the mitochondrial fatty acid oxidation derangement and kidney injury. *Front Physiol, 11*, 794. doi:10.3389/fphys.2020.00794

Cummings, B. S., & Schnellmann, R. G. (2004). Measurement of cell death in mammalian cells. *Curr Protoc Pharmacol, Chapter 12*, Unit 12 18. doi:10.1002/0471141755.ph1208s25

De Pascalis, A., Cianciolo, G., Capelli, I., Brunori, G., & La Manna, G. (2021). SGLT2 inhibitors, sodium and off-target effects: an overview. *J Nephrol, 34*(3), 673-680. doi:10.1007/s40620-020-00845-7

DeFronzo, R. A., Norton, L., & Abdul-Ghani, M. (2017). Renal, metabolic and cardiovascular considerations of SGLT2 inhibition. *Nat Rev Nephrol, 13*(1), 11-26. doi:10.1038/nrneph.2016.170

Ding, W., Yousefi, K., Goncalves, S., Goldstein, B. J., Sabater, A. L., Kloosterboer, A., . . . Shehadeh, L. A. (2018). Osteopontin deficiency ameliorates Alport pathology by preventing tubular metabolic deficits. *JCI Insight, 3*(6). doi:10.1172/jci.insight.94818

Ducasa, G. M., Mitrofanova, A., Mallela, S. K., Liu, X., Molina, J., Sloan, A., . . . Fornoni, A. (2019). ATP-binding cassette A1 deficiency causes cardiolipin-driven mitochondrial dysfunction in podocytes. *J Clin Invest, 129*(8), 3387-3400. doi:10.1172/JCI125316

Elmore, S. (2007). Apoptosis: a review of programmed cell death. *Toxicol Pathol, 35*(4), 495-516. doi:10.1080/01926230701320337

Ferrannini, E., Baldi, S., Frascerra, S., Astiarraga, B., Heise, T., Bizzotto, R., . . . Muscelli, E. (2016). Shift to fatty substrate utilization in response to sodium-glucose cotransporter 2 inhibition in subjects without diabetes and patients with type 2 diabetes. *diabetes, 65*(5), 1190-1195. doi:10.2337/db15-1356

Gaborit, B., Ancel, P., Abdullah, A. E., Maurice, F., Abdesselam, I., Calen, A., . . . Dutour, A. (2021). Effect of empagliflozin on ectopic fat stores and myocardial energetics in type 2 diabetes: the EMPACEF study. *Cardiovasc Diabetol, 20*(1), 57. doi:10.1186/s12933-021-01237-2

Ge, M., Molina, J., Ducasa, G. M., Mallela, S. K., Santos, J. V., Mitrofanova, A., . . . Fornoni, A. (2021). APOL1 risk variants affect podocyte lipid homeostasis and energy production in focal segmental glomerulosclerosis. *Hum Mol Genet*. doi:10.1093/hmg/ddab022

Gross, O., Kashtan, C. E., Rheault, M. N., Flinter, F., Savige, J., Miner, J. H., . . . Lennon, R. (2016). Advances and unmet needs in genetic, basic and clinical science in Alport syndrome: report from the 2015 International Workshop on Alport Syndrome. *Nephrol Dial Transplant*. doi:10.1093/ndt/gfw095

Gross, O., Licht, C., Anders, H. J., Hoppe, B., Beck, B., Tonshoff, B., . . . Weber, M. (2012). Early angiotensin-converting enzyme inhibition in Alport syndrome delays renal failure and improves life expectancy. *Kidney Int, 81*(5), 494-501. doi:10.1038/ki.2011.407

Grunfeld, J. P. (2000). Contemporary diagnostic approach in Alport's syndrome. *Ren Fail, 22*(6), 759-763.

Guzman, J., Jauregui, A. N., Merscher-Gomez, S., Maiguel, D., Muresan, C., Mitrofanova, A., . . . Fornoni, A. (2014). Podocyte-specific GLUT4-deficient mice have fewer and larger podocytes and are protected from diabetic nephropathy. *Diabetes, 63*(2), 701-714. doi:10.2337/db13-0752

Heerspink, H. J. L., Stefansson, B. V., Correa-Rotter, R., Chertow, G. M., Greene, T., Hou, F. F., . . . Investigators. (2020). Dapagliflozin in patients with chronic kidney disease. *N Engl J Med, 383*(15), 1436-1446. doi:10.1056/NEJMoa2024816

Huang, C., & Freter, C. (2015). Lipid metabolism, apoptosis and cancer therapy. *Int J Mol Sci, 16*(1), 924-949. doi:10.3390/ijms16010924

Jat, P. S., Noble, M. D., Ataliotis, P., Tanaka, Y., Yannoutsos, N., Larsen, L., & Kioussis, D. (1991). Direct derivation of conditionally immortal cell lines from an H-2Kb-tsA58 transgenic mouse. *Proc Natl Acad Sci U S A, 88*(12), 5096-5100. doi:10.1073/pnas.88.12.5096

Kang, H. M., Ahn, S. H., Choi, P., Ko, Y. A., Han, S. H., Chinga, F., . . . Susztak, K. (2015). Defective fatty acid oxidation in renal tubular epithelial cells has a key role in kidney fibrosis development. *Nat Med, 21*(1), 37-46. doi:10.1038/nm.3762

Kim, Jin-Ju, David, Judith M., Wilbon, Sydney S., Santos, Javier V., Patel, Devang M., Ahmad, Anis, . . . Fornoni, Alessia. (2021). Discoidin domain receptor 1 activation links extracellular

matrix to podocyte lipotoxicity in Alport syndrome. *EBioMedicine, 63*, 103162. doi:https://doi.org/10.1016/j.ebiom.2020.103162

Kuchay, M. S., Krishan, S., Mishra, S. K., Farooqui, K. J., Singh, M. K., Wasir, J. S., . . . Mithal, A. (2018). Effect of empagliflozin on liver fat in patients with type 2 diabetes and nonalcoholic fatty liver disease: a randomized controlled trial (E-LIFT Trial). *Diabetes Care, 41*(8), 1801-1808. doi:10.2337/dc18-0165

Liu, X., Ducasa, G. M., Mallela, S. K., Kim, J. J., Molina, J., Mitrofanova, A., . . . Fornoni, A. (2020). Sterol-O-acyltransferase-1 has a role in kidney disease associated with diabetes and Alport syndrome. *Kidney Int, 98*(5), 1275-1285. doi:10.1016/j.kint.2020.06.040

Longo, I., Porcedda, P., Mari, F., Giachino, D., Meloni, I., Deplano, C., . . . De Marchi, M. (2002). COL4A3/COL4A4 mutations: from familial hematuria to autosomal-dominant or recessive Alport syndrome. *Kidney Int, 61*(6), 1947-1956. doi:10.1046/j.1523-1755.2002.00379.x

Mabillard, H., & Sayer, J. A. (2020). SGLT2 inhibitors - a potential treatment for Alport syndrome. *Clin Sci (Lond), 134*(4), 379-388. doi:10.1042/CS20191276

McGuire, D. K., Shih, W. J., Cosentino, F., Charbonnel, B., Cherney, D. Z. I., Dagogo-Jack, S., . . . Cannon, C. P. (2021). Association of SGLT2 inhibitors with cardiovascular and kidney outcomes in patients with type 2 diabetes: A Meta-analysis. *JAMA Cardiol, 6*(2), 148-158. doi:10.1001/jamacardio.2020.4511

Merscher-Gomez, S., Guzman, J., Pedigo, C. E., Lehto, M., Aguillon-Prada, R., Mendez, A., . . . Fornoni, A. (2013). Cyclodextrin protects podocytes in diabetic kidney disease. *Diabetes*. doi:10.2337/db13-0399

Mitrofanova, A., Molina, J., Varona Santos, J., Guzman, J., Morales, X. A., Ducasa, G. M., . . . Fornoni, A. (2018). Hydroxypropyl-beta-cyclodextrin protects from kidney disease in experimental Alport syndrome and focal segmental glomerulosclerosis. *Kidney Int, 94*(6), 1151-1159. doi:10.1016/j.kint.2018.06.031

Mizoguchi, T., Edano, T., & Koshi, T. (2004). A method of direct measurement for the enzymatic determination of cholesteryl esters. *J Lipid Res, 45*(2), 396-401. doi:10.1194/jlr.D300024-JLR200

Mundel, P., Reiser, J., Zuniga Mejia Borja, A., Pavenstadt, H., Davidson, G. R., Kriz, W., & Zeller, R. (1997). Rearrangements of the cytoskeleton and cell contacts induce process formation during differentiation of conditionally immortalized mouse podocyte cell lines. *Exp Cell Res, 236*(1), 248-258. doi:10.1006/excr.1997.3739

Novikov, A., & Vallon, V. (2016). Sodium glucose cotransporter 2 inhibition in the diabetic kidney: an update. *Curr Opin Nephrol Hypertens, 25*(1), 50-58. doi:10.1097/MNH.0000000000000187

Osataphan, S., Macchi, C., Singhal, G., Chimene-Weiss, J., Sales, V., Kozuka, C., . . . Patti, M. E. (2019). SGLT2 inhibition reprograms systemic metabolism via FGF21-dependent and -independent mechanisms. *JCI Insight, 4*(5). doi:10.1172/jci.insight.123130

Pedigo, C. E., Ducasa, G. M., Leclercq, F., Sloan, A., Mitrofanova, A., Hashmi, T., . . . Fornoni, A. (2016). Local TNF causes NFATc1-dependent cholesterol-mediated podocyte injury. *J Clin Invest, 126*(9), 3336-3350. doi:10.1172/JCI85939

Romani, P., Brian, I., Santinon, G., Pocaterra, A., Audano, M., Pedretti, S., . . . Dupont, S. (2019). Extracellular matrix mechanical cues regulate lipid metabolism through Lipin-1 and SREBP. *Nat Cell Biol, 21*(3), 338-347. doi:10.1038/s41556-018-0270-5

Ross, B. D., Espinal, J., & Silva, P. (1986). Glucose metabolism in renal tubular function. *Kidney Int, 29*(1), 54-67. doi:10.1038/ki.1986.8

Shibuya, T., Fushimi, N., Kawai, M., Yoshida, Y., Hachiya, H., Ito, S., . . . Mori, A. (2018). Luseogliflozin improves liver fat deposition compared to metformin in type 2 diabetes patients with non-alcoholic fatty liver disease: A prospective randomized controlled pilot study. *Diabetes Obes Metab, 20*(2), 438-442. doi:10.1111/dom.13061

Takahashi, N., Boysen, G., Li, F., Li, Y., & Swenberg, J. A. (2007). Tandem mass spectrometry measurements of creatinine in mouse plasma and urine for determining glomerular filtration rate. *Kidney Int, 71*(3), 266-271. doi:10.1038/sj.ki.5002033

Terryn, S., Jouret, F., Vandenabeele, F., Smolders, I., Moreels, M., Devuyst, O., . . . Van Kerkhove, E. (2007). A primary culture of mouse proximal tubular cells, established on collagen-coated membranes. *Am J Physiol Renal Physiol, 293*(2), F476-485. doi:10.1152/ajprenal.00363.2006

Vallon, V., Platt, K. A., Cunard, R., Schroth, J., Whaley, J., Thomson, S. C., . . . Rieg, T. (2011). SGLT2 mediates glucose reabsorption in the early proximal tubule. *J Am Soc Nephrol, 22*(1), 104-112. doi:10.1681/ASN.2010030246

Vallon, V., & Thomson, S. C. (2017). Targeting renal glucose reabsorption to treat hyperglycaemia: the pleiotropic effects of SGLT2 inhibition. *Diabetologia, 60*(2), 215-225. doi:10.1007/s00125-016-4157-3

Wallenius, K., Kroon, T., Hagstedt, T., Lofgren, L., Sorhede-Winzell, M., Boucher, J., . . . Oakes, N. D. (2022). The SGLT2 inhibitor dapagliflozin promotes systemic FFA mobilization, enhances hepatic beta-oxidation, and induces ketosis. *J Lipid Res, 63*(3), 100176. doi:10.1016/j.jlr.2022.100176

Wang, X. X., Levi, J., Luo, Y., Myakala, K., Herman-Edelstein, M., Qiu, L., . . . Levi, M. (2017). SGLT2 protein expression is increased in human diabetic nephropathy: SGLT2 protein inhibition decreases renal lipid accumulation, inflammation, and the development of nephropathy in diabetic mice. *J Biol Chem, 292*(13), 5335-5348. doi:10.1074/jbc.M117.779520

Wei, D., Liao, L., Wang, H., Zhang, W., Wang, T., & Xu, Z. (2020). Canagliflozin ameliorates obesity by improving mitochondrial function and fatty acid oxidation via PPARalpha in vivo and in vitro. *Life Sci, 247*, 117414. doi:10.1016/j.lfs.2020.117414

Williamson, D. A. (1961). Alport's syndrome of hereditary nephritis with deafness. *Lancet, 2*(7216), 1321-1323.

Wright, M. B., Varona Santos, J., Kemmer, C., Maugeais, C., Carralot, J. P., Roever, S., . . . Fornoni, A. (2021). Compounds targeting OSBPL7 increase ABCA1-dependent cholesterol efflux preserving kidney function in two models of kidney disease. *Nat Commun, 12*(1), 4662. doi:10.1038/s41467-021-24890-3

Yokono, M., Takasu, T., Hayashizaki, Y., Mitsuoka, K., Kihara, R., Muramatsu, Y., . . . Uchiyama, Y. (2014). SGLT2 selective inhibitor ipragliflozin reduces body fat mass by increasing fatty acid oxidation in high-fat diet-induced obese rats. *Eur J Pharmacol, 727*, 66-74. doi:10.1016/j.ejphar.2014.01.040

Yoo, T. H., Pedigo, C. E., Guzman, J., Correa-Medina, M., Wei, C., Villarreal, R., . . . Merscher, S. (2015). Sphingomyelinase-like phosphodiesterase 3b expression levels determine podocyte injury phenotypes in glomerular disease. *J Am Soc Nephrol, 26*(1), 133-147. doi:10.1681/ASN.2013111213

Zhang, S., Hulver, M. W., McMillan, R. P., Cline, M. A., & Gilbert, E. R. (2014). The pivotal role of pyruvate dehydrogenase kinases in metabolic flexibility. *Nutr Metab (Lond), 11*(1), 10. doi:10.1186/1743-7075-11-10

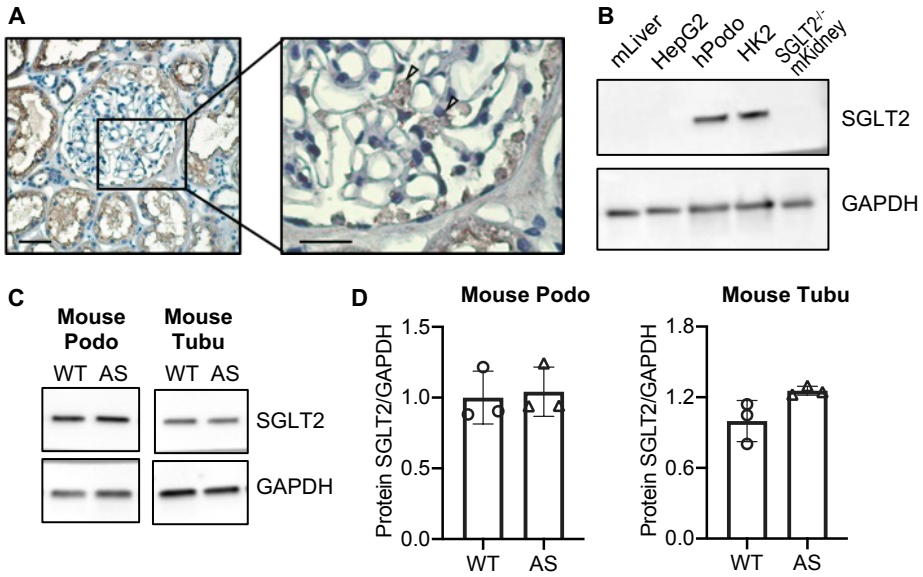

Figure 1. SGLT2 protein is expressed in human kidney cortex and in cultured human and mouse podocytes. (**A**) Immunohistochemistry staining of human kidney cortex for SGLT2 (left panel, scale bar: 50 μm; right panel, scale bar: 25 μm). (**B**) Western blot images demonstrating SGLT2 expression in cultured human podocytes (hPodo). Mouse liver lysate (mLiver), HepG2 liver cancer cells and kidney lysate from SGLT2$^{-/-}$ mouse (SGLT2$^{-/-}$ mKidney) were used as the negative controls. HK2 proximal tubular cells were used as the positive control. (**C, D**) Western blot images (C) and quantification (D) demonstrating SGLT2 expression in mouse proximal tubular cells (Tubu) and podocytes (Podo) established from wildtype (WT) and Alport (AS) mice (n = 3). Two-tailed Student's t-test.

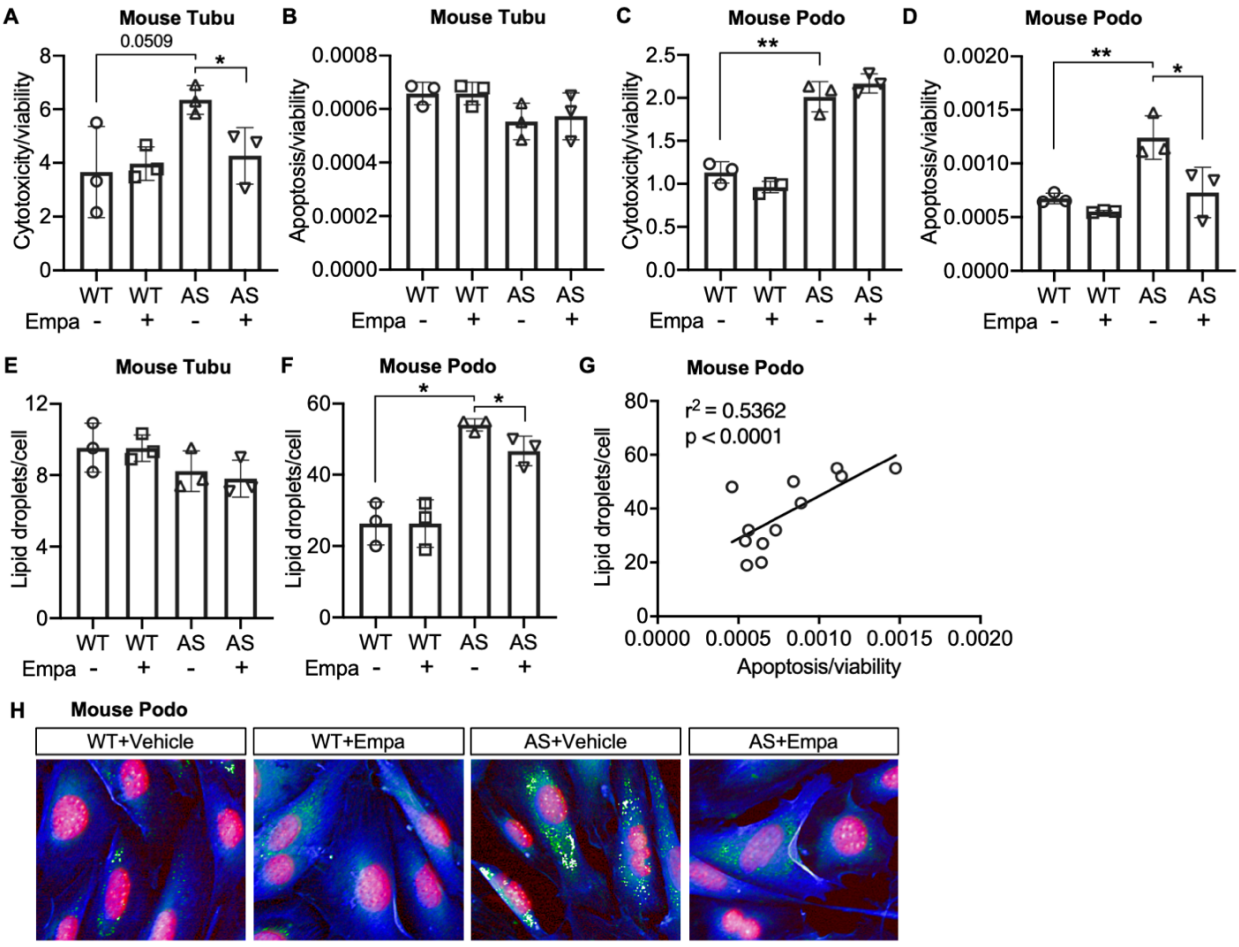

Figure 2. Treatment of AS podocytes with empagliflozin reduces lipid droplet (LD) accumulation and apoptosis. (**A**-**D**) Immortalized podocytes and tubular cells of WT and AS mice treated with empagliflozin (Empa) or vehicle for 48 hours. (**A**,**C**) Bar graph analysis showing cytotoxicity normalized to viability (n = 3). (**B**,**D**) Bar graph analysis showing apoptosis normalized to viability (n = 3). (**E**,**F**) LD accumulation in tubular cells (**E**) and podocytes (**F**) was measured by Nile red staining. Bar graph analysis showing the quantification of the number of LDs per cell (n = 3). (**G**) Correlation analyses between the LD accumulation and apoptosis in podocytes (n = 12). (**H**) Representative images of Nile red staining demonstrate increased LD numbers (Nile red: green) in AS podocytes (Cell mask blue: blue; DAPI: red) compared to WT podocytes, which is reduced by Empa treatment. **A**-**F**, Two-tailed Student's t-test. **G**, Pearson's correlation coefficient. **p* < 0.5, ***p* < 0.01.

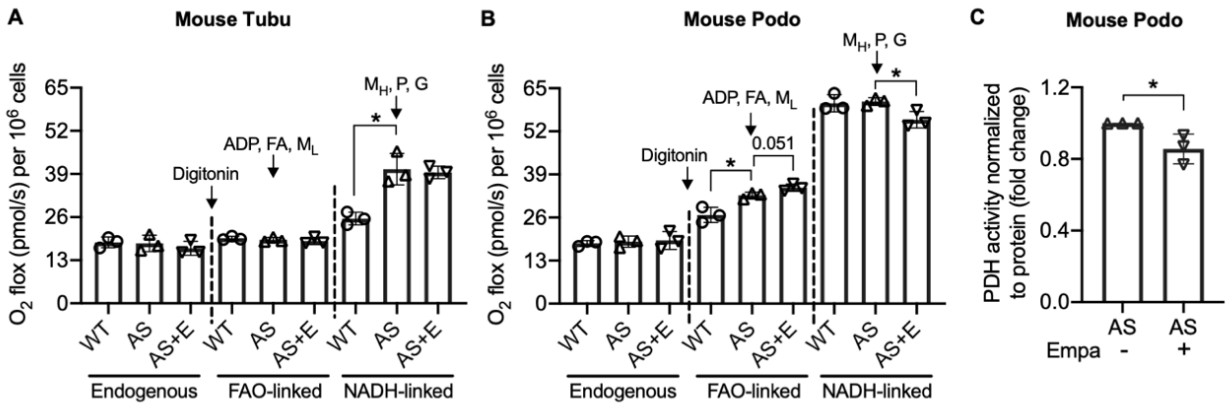

Figure 3. Empagliflozin inhibits the utilization of pyruvate as a metabolic substrate in AS podocytes. (**A**, **B**) Bar graph analysis of endogenous and substrate-driven oxygen consumption rates in wildtype (WT) and Alport (AS) tubular cells (**A**) and podocytes (**B**) treated with or without empagliflozin (E) (n = 3). The sequential addition of permeabilizing agent and substrates was labeled in the figure. (**C**) Pyruvate dehydrogenase (PDH) activity was measured by a colorimetric assay in protein extracts from AS podocytes, normalized to protein concentration (n = 3). Two-tailed Student's t-test, *$p < 0.5$. FA: octanoylcarnitine; M_L: malate-low concentration; M_H: malate-high concentration; P: pyruvate; G: glutamate.

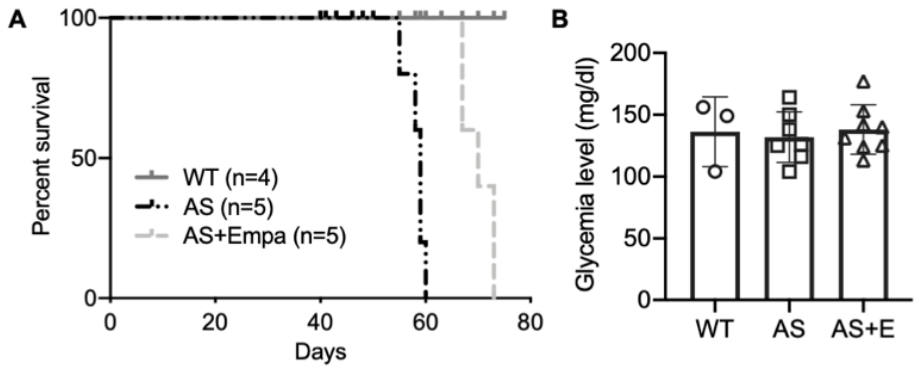

Figure 4. Empa improves the survival of AS mice. (**A**) Survival curve (n = 4-5) of AS mice fed empagliflozin-supplemented (E) chow versus placebo diet starting at 4 weeks of age, compared to age-matched WT control mice. (**B**) Glycemia levels of WT and AS mice fed placebo diet and AS mice fed empagliflozin chow (n = 3-7). **B**, AS vs AS+E: Two-tailed Student's t-test.

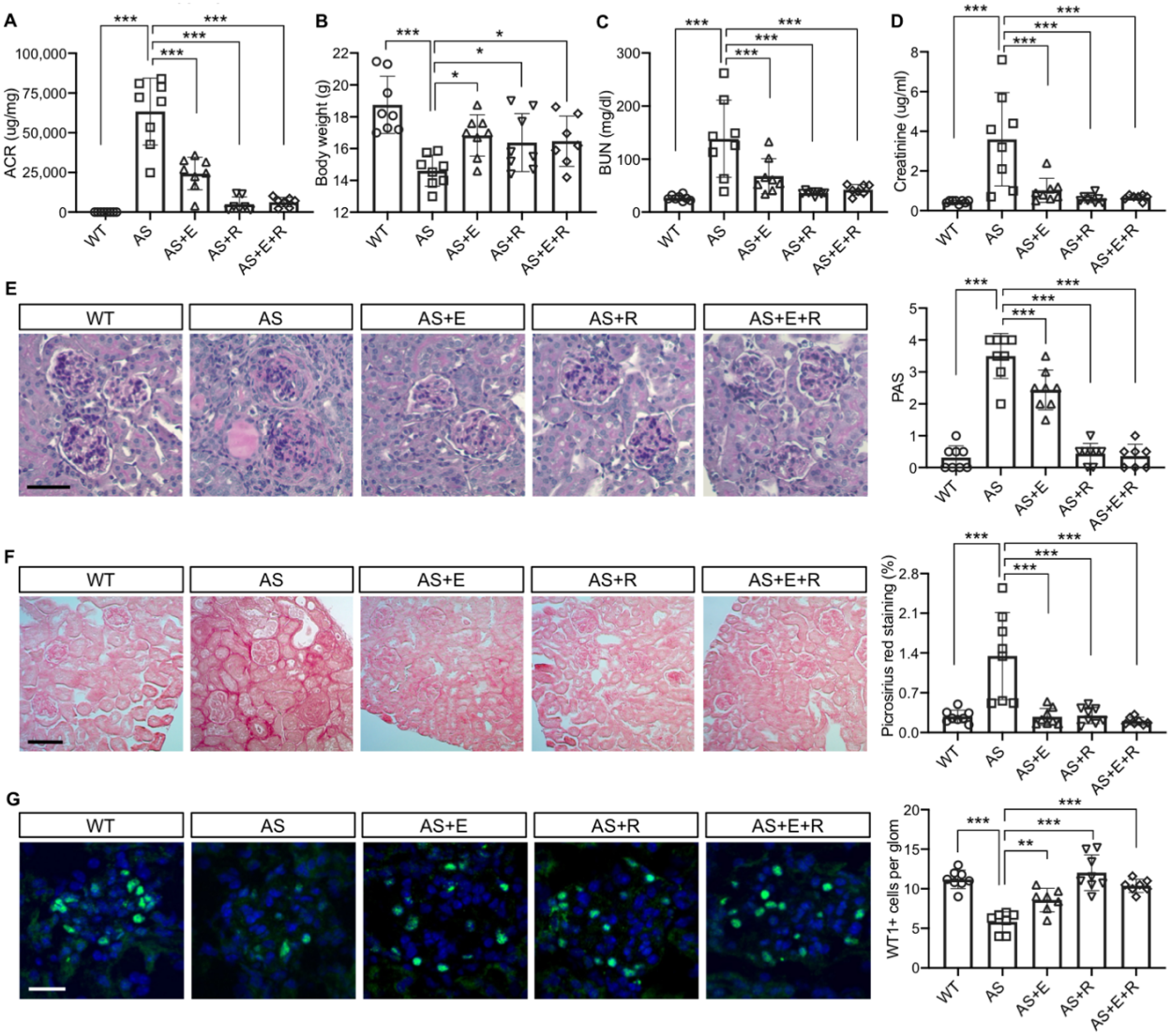

Figure 5. Empagliflozin improves renal function in a mouse model of Alport syndrome. (**A**) Urinary albumin-to-creatinine ratio (ACR) in WT and AS mice fed with placebo, empagliflozin (E), ramipril (R), or the combination of empagliflozin and ramipril (E+R). Urines were collected at the time of sacrifice (n = 7-8). (**B**) Bar graph analysis of body weights of mice from all experimental groups. (**C**,**D**) Bar graph analysis of blood urea nitrogen (BUN) (**C**) and creatinine (**D**) levels of mice from all experimental groups (n = 7-8). (**E**) Representative images of Periodic acid-Schiff (PAS) staining and bar graph analysis showing the mesangial expansion score of kidney cortices sections (scale bar: 50 µm; n = 7-8). (**F**) Representative Picrosirius red staining and bar graph

analysis showing the quantification of fibrosis in kidney cortices sections (scale bar: 100 µm; n= 7-8). (**G**) Representative images of kidney cortices stained with WT1 (green) to detect podocytes and DAPI (blue) to reveal nuclei and bar graph quantification of the average number of WT1-positive podocytes per glomerulus (scale bar: 25 µm, n = 7-8). One-Way ANOVA followed by Holm-Sidak's multiple comparison. *$p < 0.05$, **$p < 0.01$, ***$p < 0.001$.

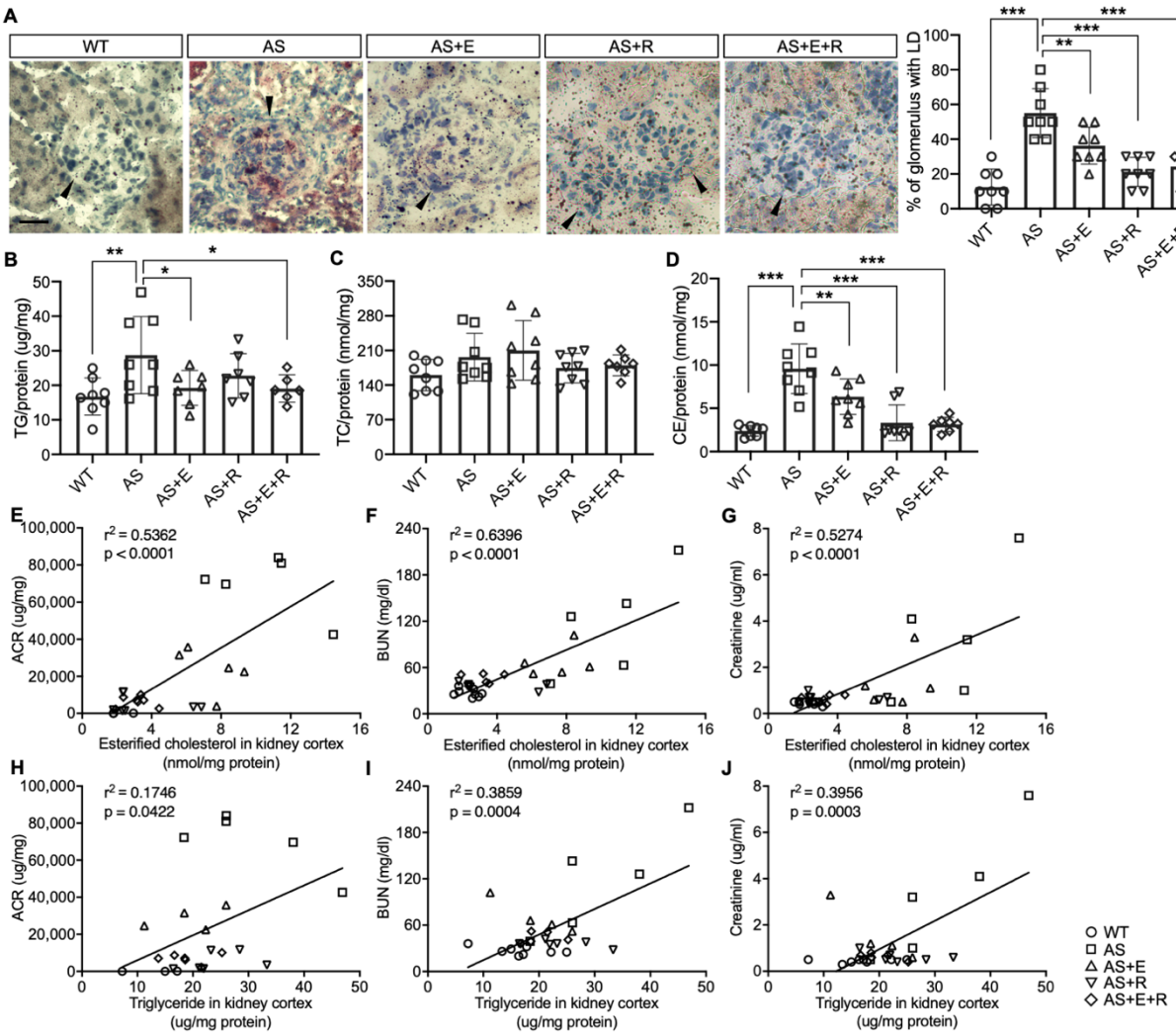

Figure 6. Empagliflozin prevents renal lipid accumulation in experimental Alport syndrome. (**A**) Representative Oil Red-O (ORO) images of stained kidney cortices sections (scale bar: 20 μm) and bar graph quantification of the number of glomeruli with lipid droplets (LD) in ORO-stained slides (n = 7-8). (**B**-**D**) Bar graph analysis of triglyceride (TG, **B**), total cholesterol (TC, **C**), and cholesterol ester (CE, **D**) contents in kidney cortices. Values are normalized to protein concentrations (n = 6-8). (**E**-**G**) Correlation analyses between the CE content of kidney cortices and ACR, BUN or creatinine (n = 27, 31, 31). (**H**-**J**) Correlation analyses between the TG content of kidney cortices and ACR, BUN or creatinine (n = 29, 29, 29). **A**-**D**, One-Way ANOVA

followed by Holm-Sidak's multiple comparison. **E-J**, Pearson's correlation coefficient. *$p < 0.05$, **$p < 0.01$, ***$p < 0.001$.

SUPPLEMENTAL FIGURES

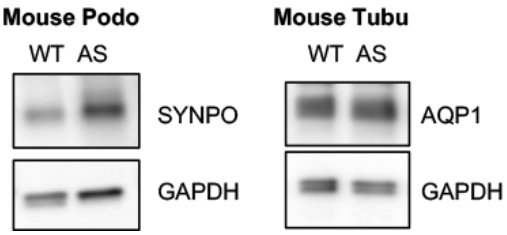

Figure 1 - Figure supplement 1. Podocyte-specific marker Synaptopodin (SYNPO) and tubule-specific marker Aquaporin 1 (AQP1) was confirmed in podocyte and tubular cell lines, respectively.

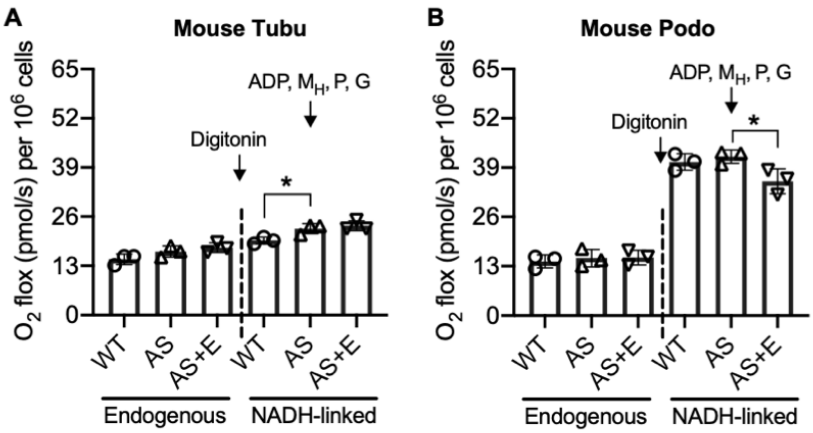

Figure 3 - Figure supplement 1. Empagliflozin inhibits NADH-linked oxygen consumption rate in AS podocytes. (A, B) Bar graph analysis of endogenous and substrate-driven oxygen consumption rates in wildtype (WT) and Alport (AS) tubular cells (A) and podocytes (B) treated with or without empagliflozin (E) (n=3). The sequential addition of permeabilizing agent and substrates was labeled in the figure. Two-tailed Student's t-test, $*p < 0.5$. M_H: malate-high concentration; P: pyruvate; G: glutamate.